Coastal Engineering 57 (2010) 52–61

Contents lists available at ScienceDirect

Coastal Engineering

journal homepage: www.elsevier.com/locate/coastaleng

Estimation of infragravity waves at intermediate water depth

A.J.H.M. Reniers [a,c,*], M.J. Groenewegen [a,d], K.C. Ewans [b], S. Masterton [b], G.S. Stelling [a], J. Meek [a]

[a] Delft University of Technology, Delft, The Netherlands
[b] Shell Int. Exploration & Production, Rijswijk, Netherlands
[c] Rosenstiel School of Marine and Atmospheric Science, University of Miami, USA
[d] Roland Berger, Amsterdam, The Netherlands

ARTICLE INFO

Article history:
Received 25 January 2008
Received in revised form 9 September 2009
Accepted 25 September 2009
Available online 5 November 2009

Keywords:
Infragravity waves
Numerical predictions
Vessel motions

ABSTRACT

The accuracy of nearshore infragravity wave height model predictions has been investigated using a combination of the spectral short wave evolution model SWAN and a linear 1D SurfBeat model (IDSB). Data recorded by a wave rider located approximately 3.5 km from the coast at 18 m water depth have been used to construct the short wave frequency-directional spectra that are subsequently translated to approximately 8 m water depth with the third generation short wave model SWAN. Next the SWAN-computed frequency-directional spectra are used as input for IDSB to compute the infragravity response in the 0.01 Hz–0.05 Hz frequency range, generated by the transformation of the grouped short waves through the surf zone including bound long waves, leaky waves and edge waves at this depth. Comparison of the computed and measured infragravity waves in 8 m water depth shows an average skill of approximately 80%. Using data from a directional buoy located approximately 70 km offshore as input for the SWAN model results in an average infragravity prediction skill of 47%. This difference in skill is in a large part related to the under prediction of the short wave directional spreading by SWAN. Accounting for the spreading mismatch increases the skill to 70%. Directional analyses of the infragravity waves shows that outgoing infragravity wave heights at 8 m depth are generally over predicted during storm conditions suggesting that dissipation mechanisms in addition to bottom friction such as non-linear energy transfer and long wave breaking may be important. Provided that the infragravity wave reflection at the beach is close to unity and tidal water level modulations are modest, a relatively small computational effort allows for the generation of long-term infragravity data sets at intermediate water depths. These data can subsequently be analyzed to establish infragravity wave height design criteria for engineering facilities exposed to the open ocean, such as nearshore tanker offloading terminals at coastal locations.

1. Introduction

Infragravity waves have periods between 25 s and 250 s and are generated by the groupiness of the incident waves. Infragravity waves can have significant influence in several areas. The importance of incorporating infragravity waves in shallow water to calculate moored LNG carrier motions is shown by Naciri et al. (2004). In addition, van der Molen (2006) and van der Molen et al. (2006) have shown the importance of harbor resonance in relation to moored vessel motions due to infragravity waves with a period between 30 and 300 s. Roelvink and Stive (1989) have shown the importance with respect to morphology where the coupling between the wave groups and the underlying infragravity waves results in preferential sediment transport directions. Other important areas are wave runup (van Gent, 2001), dune erosion (van Thiel de Vries et al., 2008; Roelvink et al., 2009) and over wash (McCall et al., 2009).

The first observations where infragravity waves were linked to surface elevations on a wave group scale were done by Munk (1949) and Tucker (1950). The latter observed a significant positive correlation at a negative time lag and observed a smaller negative correlation at zero time lag. Biesel (1952) showed that bound infragravity waves propagate with the group velocity of the short wave groups with a phase lag of 180° thus explaining the negative correlation at zero time lag. Longuet-Higgins and Stewart (1962, 1964) found a possible explanation for the larger positive correlation at negative time lag suggesting that bound infragravity waves, non-linearly forced by the spatial changes of short wave momentum flux, increase strongly in amplitude while traveling with the shoaling wave groups to the shore. These bound infragravity waves then get released at breaking and subsequently reflect at the shore line towards deeper water as free infragravity waves experiencing weaker inverse shoaling. Due to the stronger refraction of the free infragravity waves not all reflected infragravity waves propagate to the deeper water, but some

* Corresponding author. Delft University of Technology, Delft, The Netherlands.
E-mail address: A.J.H.M.Reniers@tudelft.nl (A.J.H.M. Reniers).

0378-3839/$ – see front matter © 2009 Elsevier B.V. All rights reserved.
doi:10.1016/j.coastaleng.2009.09.013

refract back to the shore where reflection takes place again (Herbers et al., 1995a). The infragravity waves that make it out to deeper water are called leaky waves, whereas the trapped waves are called edge waves (Ursell, 1952).

Reniers et al. (2002) presented a linear model to compute infragravity waves over arbitrary alongshore uniform bottom profiles including bound, leaky and edge waves in the near shore zone. This 1D SurfBeat (IDSB) model is able to give estimates of infragravity wave conditions based on directional short wave data defined at the sea boundary of the computational area. The infragravity wave response is calculated using linear shallow water equations, taking into account the presence of bottom friction, set-up of the mean water level and rollers.

For practical applications it is interesting to use existing short wave data recorded offshore to compute infragravity waves near shore instead of recording new infragravity wave data. The large sets of short wave data recorded over the last decades can then be used to compute infragravity waves over many kilometers along coastal zones. To that end the offshore wave conditions have to be translated to the seaward offshore boundary condition of the infragravity model. This operation can be performed with a spectral short wave model such as SWAN (Booij et al., 1999; Ris et al., 1999), resolving the frequency-directional distribution of the incident waves which is important in the forcing of the infragravity response (Herbers et al., 1994, 1995a). The combination of a spectral short wave model and IDSB can then be used for infragravity wave predictions based on new or existing short wave data records further offshore. This technique can easily be extended by coupling a regional spectral short wave model to a global wave model to yield the boundary conditions for the infragravity modeling at an arbitrary location. In this study data recorded with a directional buoy offshore of Duck (NC), located approximately 3.5 km from the coast at 18 m water depth have been used to compute the infragravity waves near shore. The results have been compared to data recorded at the FRF (Field Research Facility) array at 8 m water depth.

The objective of this study is to examine the accuracy of the predictions of the root mean square infragravity wave heights at intermediate water depth (O(8)m) computed with the combination SWAN–IDSB using one month of wave data covering a wide range in wave conditions. If satisfactory, there is a potential for this combination of models to be used to generate infragravity wave statistics at locations of interest along the coast that in turn can for instance be used to assess ship motions and expected down time.

In the following, a brief description of the model set-up is given followed by the comparison of the computed and measured short waves and infragravity waves. In the discussion, the present results are put in perspective, and this is followed by conclusions.

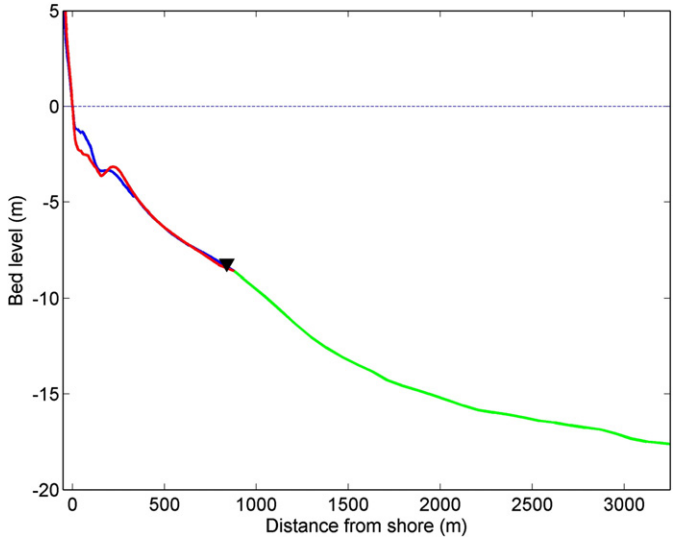

Fig. 1. Bottom profiles used in the model calculations. Directional spectra are translated from the Waverider buoy location (18 m water depth) to 8.8 m water depth with SWAN using the offshore bottom profile (solid green line). Infragravity waves are calculated at the 8 m-array (indicated by the black triangle) with IDSB using the 97 Sandy Duck profile (solid blue line). The March 05 bottom profile (red solid line) is used in sensitivity calculations.

2. Model set-up

To verify the capability to predict infragravity waves by using the combination SWAN–IDSB, wave data recorded by the Field Research Facility (FRF) near Duck, North Carolina USA, have been used. The datasets have been recorded at two locations during April 2005. One dataset contains time series of vertical and horizontal accelerations recorded by a directional Waverider buoy at a depth of approximately 18 m. The other set contains time series of pressures recorded by 15 pressure gauges spread over an alongshore and a cross-shore array at a depth of approximately 8 m (Fig. 1). The month of April has been chosen for the comparison because it contains both modest wave conditions and a severe storm with significant wave heights of 4.5 m.

The data recorded offshore by the directional buoy are translated into directional spectra by applying the Maximum Entropy Method (MEM) (Lygre and Krogstad, 1986). Samples of 1600 s (available every half hour), considered to represent a steady sea state, are translated into frequency-directional spectra with a frequency resolution of 0.005 Hz between 0.05 Hz and 0.31 Hz. The corresponding directional distribution over 360° has a resolution of 3.6°. The frequency-directional spectra are translated to the most offshore FRF array sensor location at a water depth of 8.8 m using 1D–SWAN, thus assuming locally alongshore uniform conditions (in reality the buoy was situated 4.1 km further down the coast at the same depth).

The 2 h and 16 min long pressure records from the FRF array (available every 3 h) are translated into surface elevation records using linear wave theory. To reduce the influence of the noise at the higher frequencies, the transfer function is set to a maximum of 2.5. The time series are used to calculate the frequency-directional (f–θ) infragravity spectra with the Maximum Likelihood Estimator (MLE, Davis and Regier 1977; Pawka, 1983, see Appendix A for details). Next the variance densities in the low frequency range (0.01 Hz–0.05 Hz) of these spectra are used to derive the total, the incoming ($-90° < \theta_{in} < +90°$) and outgoing ($\theta_{out} < -90°$ or $\theta_{out} > 90°$) root mean square low frequency wave heights:

$$H_{rms,lo,tot} = 2\sqrt{2}\int_{\theta_{all}}\int_{0.01Hz}^{0.05Hz} E_{\eta\eta}(f,\theta)dfd\theta \quad (1a)$$

$$H_{rms,lo,in} = 2\sqrt{2}\int_{\theta_{in}}\int_{0.01Hz}^{0.05Hz} E_{\eta\eta}(f,\theta)dfd\theta \quad (1b)$$

$$H_{rms,lo,out} = 2\sqrt{2}\int_{\theta_{out}}\int_{0.01Hz}^{0.05Hz} E_{\eta\eta}(f,\theta)dfd\theta \quad (1c)$$

where $\theta = 0$ corresponds to normal incidence. A lower frequency limit of 0.01 Hz is chosen due to the fact that at frequencies less than 0.01 Hz the correlation between the observed infragravity response and the incident wave conditions drops off (Okihiro and Guza, 1995; Herbers et al., 1995b), suggesting that these motions originate from other (remote) sources not captured by the present modeling set-up.

IDSB uses the SWAN output spectra to calculate the infragravity waves at the FRF array which is then compared with the observed root mean square infragravity wave heights obtained from the pressure records.

The 1D–SWAN wave transformation is performed for the incident waves without wind forcing, tidal motions and set-up but does include shoaling, refraction, depth induced wave breaking, bottom friction and triad interactions. The output of SWAN is a frequency-directional spectrum containing 40 intervals with a logarithmic scale in the frequency domain between 0.05 Hz and 0.31 Hz. The directional distribution is divided into 51 steps of each 7.06°. The 1D bathymetry used in this translation is based on surveys done in 1999 and 2000 (Fig. 1). The JONSWAP friction parameter taken into account in the SWAN computation is 0.038 m^2/s^3 based on dominating swell waves during the storm conditions in April 2005 (Hasselmann et al., 1973).

The wave breaking parameters used in SWAN are the proportionality coefficient of the rate of dissipation, α, and the maximum individual wave height over depth, γ, with values of 1.0 and 0.73 respectively. The triad parameters used in the LTA method (Eldeberky, 1996) are a scaling coefficient, the maximum considered frequency, the critical Ursell number appearing in the expression for the bi-phase, and the lower threshold for the Ursell number, and are set at their default values of 0.1, 2.2 Hz, 0.2, and 0.01 respectively.

The SWAN-derived output spectra are interpolated to yield a frequency resolution of 0.01 Hz between 0.05 Hz and 0.31 Hz and a directional resolution of 2.5° between plus and minus 72° (thus restricted to incident waves only) and used as input for the IDSB computations. The IDSB computational cross-shore grid has a resolution of 4 m. The 1D bathymetry from the shore to the eight meter array (Fig. 1) is the same as used by Reniers et al. (2004) and originates from the Sandy Duck experiment from 1997. The friction parameter, and the parameters to calculate the transformation of the spectral variance density from the sea boundary to the shore and the accompanying set-up of the mean water level are kept the same compared to the study done at Duck by Reniers et al. (2002). Based on this study a relation between the significant wave height and the optimal wave breaking saturation parameter gamma for the dissipation formulation of Roelvink (1993) has been derived consistent with recent model calibrations carried out by Apotsos et al. (2008) which has been used in the present IDSB computations:

$$\gamma = 0.41 + 0.19 \tan h(0.33 Hm0_0) \quad (2)$$

where $Hm0_0$ represents the incident significant wave height at deep water.

The boundary conditions for the infragravity wave calculations account for the incoming bound infragravity waves, the outgoing free infragravity waves and edge waves at the sea boundary, and a 100% reflection of infragravity waves at the shore line, where a minimum computational water depth of 0.1 m is applied. IDSB subsequently calculates the infragravity surface elevation at the individual sensor positions of the FRF array to which the MLE method is applied to derive the model-predicted frequency-directional infragravity spectrum and corresponding total, incoming and outgoing infragravity wave heights for each offshore incident wave condition following Eq. (1).

3. Comparison with measured values

3.1. 1D–SWAN wave transformation

As a first step in the model verification the output of SWAN is compared with the directional spectra at the 8-meter array published by the US Army FRF Centre. All comparisons are made at the three-hour FRF interval time scale. The skill defined as (Gallagher et al., 1998):

$$skill = 1 - \frac{\sqrt{(M_i - C_i)^2}}{\sqrt{M_i^2}} \quad (3)$$

is used to quantify the accuracy of the predictions, C, compared to the measured values, M, for each offshore wave condition measured at 18 m water depth (denoted by the subscript i). The infragravity wave response depends on the incident wave height (higher waves equals stronger forcing), the mean direction (obliquely incident waves force more edge waves), the mean period (longer period waves result in stronger forcing), and directional spreading (more spreading results in weaker forcing). The comparisons of these four key parameters are shown in Fig. 2; the mean skills are denoted between brackets: Hm0 (0.84), mean frequency (0.95), mean direction (0.98) and spreading (0.92) (according to Kuik et al., 1988). The generally higher Hm0 values obtained from the 2D variance density spectra from the FRF Centre have been recalculated with a FFT calculation applied on the time series of the gauge with the same water depth as the SWAN output. This comparison has a mean skill of 0.88 and shows a better agreement overall.

The comparisons (Fig. 2) show that the MEM-based frequency-directional spectra obtained from the Waverider buoy time series in combination with the transformation to the array location using 1D–SWAN gives accurate incident wave conditions at the array location, confirming correct treatment of the measured Waverider buoy data and SWAN model implementation. The corresponding spectra can now be used as input to IDSB to calculate the infragravity wave response. The calculated root mean square infragravity wave heights are compared with measurements at the array location presented next.

4. IDSB infragravity response

The infragravity response within the nearshore is calculated for the period of the month of April 2005. The MLE method is applied to both the measured FRF array and corresponding IDSB model-predicted surface elevation time series (see Appendix A for details).

The frequency–integrated directional infragravity spectra during the month of April clearly show the response to the individual storm events in both the observations and model predictions (compare panels A and B in Fig. 3 with the upper panel in Fig. 2). The infragravity energy density is typically centred around the shore normal axis ($\theta = 0^o$ and $\theta = +/-180^o$) although at times there is a predominance of alongshore propagating edge waves forced by obliquely incident short waves (indicated by the green dots in Figs. 2 and 3). Comparison with the observations shows good correspondence for the incoming infragravity wave height (panel D of Fig. 3), skill = 0.82 and a root mean square error, ε, of 1 cm, and generally an over prediction of the outgoing infragravity wave height during storm conditions (panel E of Fig. 3), resulting in a lower skill = 0.66 and larger error $\varepsilon = 2$ cm. The skill for the total infragravity wave height is 0.82 with $\varepsilon = 1.5$ cm (panel C of Fig. 3).

The directional spreading as defined by Kuik et al. (1988) is evaluated for both the incoming and outgoing infragravity waves, where the mean direction corresponds to the first order moment of the infragravity directional spectrum. Model-predicted and observed mean directions for incoming and outgoing infragravity waves are generally closely aligned with the shore normal and correspond to the mean direction of the incident waves (compare panels A and C in Fig. 4 with panel C in Fig. 2). Infragravity-directional spreading is much broader than the incident wave spreading (compare panels B and D in Fig. 4 with panel D in Fig. 2) consistent with earlier observations and theory (Herbers et al., 1995b; Sand, 1982). The directional spreading for the model-predicted incident infragravity waves is generally broader than observed (Panel B in Fig. 4 and Panel A in Fig. 3), which may be related to the over-estimation of the bound long wave contribution for larger difference angles (Fig. C1 in Reniers et al., 2002). Predicted directional spreading of the outgoing infragravity waves is in good agreement with the observations (panel D in Fig. 4).

The natural period of a moored ship is expected to be in the lower regions of the infragravity frequency domain. To that end two

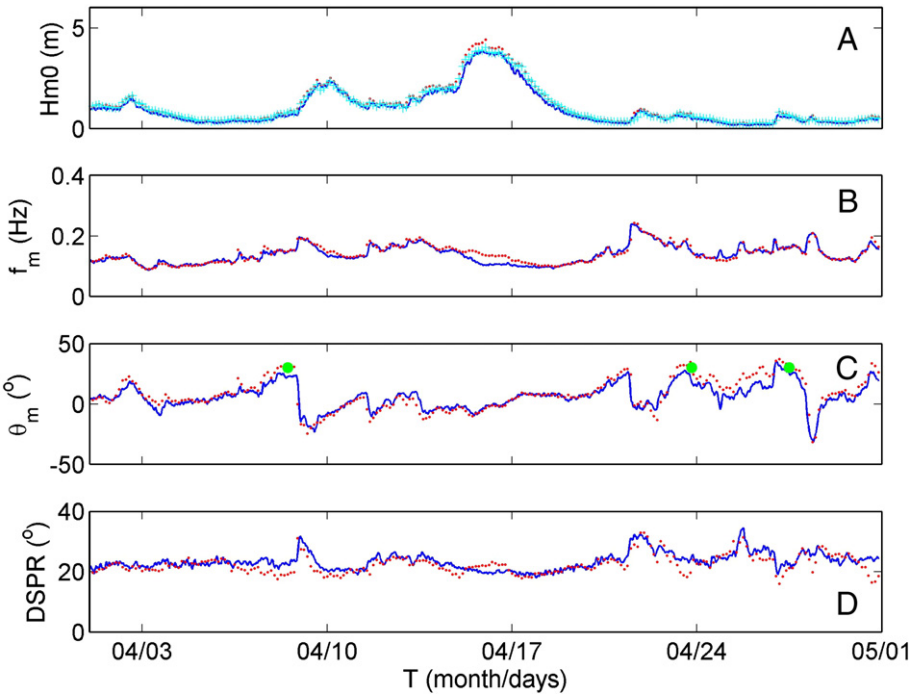

Fig. 2. Comparisons between 1D-SWAN output at 8.8 m water depth and FRF data published on the website at 8 m-array location. Panel A: Hm0 computed with SWAN (solid), FRF data (•) and a FFT computation at 8.8 m water depth (+). Panel B: Mean frequency computed with SWAN (solid) and FRF data (•). Panel C: Mean incidence angle (0° is shore normal) computed with SWAN (solid) and FRF data (•). Green dots indicate times of edge wave predominance. Panel D: Circular root mean square spreading computed with SWAN (solid) and FRF data (•).

separate frequency intervals have been defined: 0.01 Hz–0.03 Hz and 0.03 Hz–0.05 Hz respectively. Predicted energy density levels in the 0.01 Hz–0.03 Hz frequency range correspond well with the observations (panels A and B of Fig. 5). As a result the corresponding total infragravity root mean square wave height compares well with the measured values in this frequency domain (panel C in Fig. 5) and the over-estimation of the total root mean square wave heights during the storms is no longer present. This is partly a result of the combined

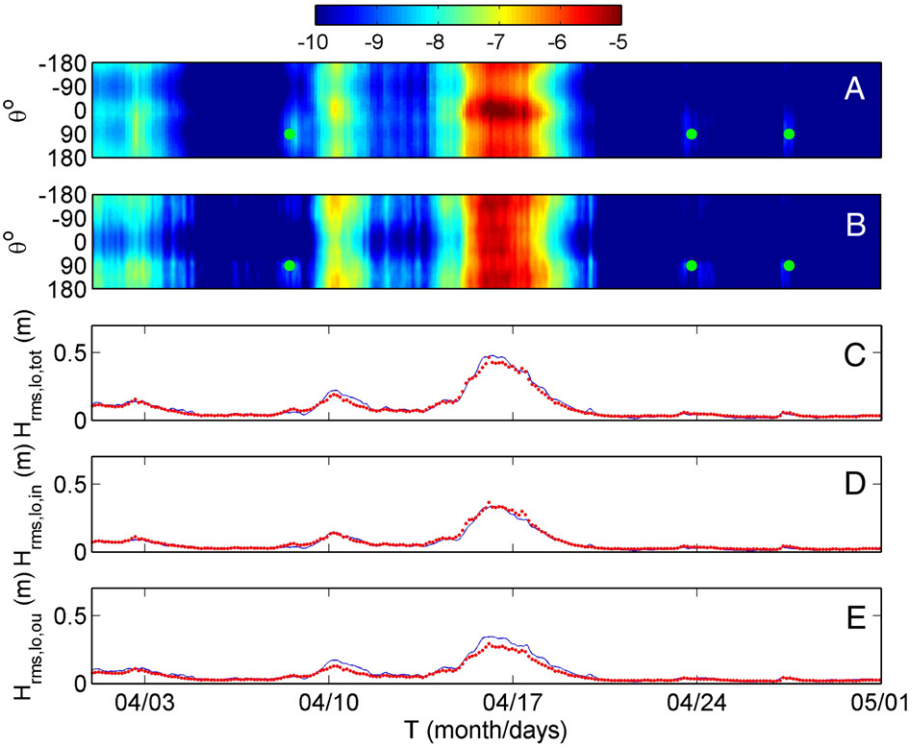

Fig. 3. Infragravity conditions during April 2005 at the 8 m-array location. Panel A: Observed 0.01 Hz – 0.05 Hz frequency-integrated directional infragravity spectra. Panel B: Similar for predicted directional infragravity spectra. Green dots indicate times of edge wave predominance. Panel C: Observed (red dots) and predicted (solid line) total infragravity root mean square wave height. Panel D: Incoming infragravity root mean square wave height. Panel E: Outgoing infragravity root mean square wave height.

small underestimation of the incoming infragravity waves and small over prediction of the outgoing infragravity waves within this frequency band during storm conditions (panels D and E in Fig. 5).

The accuracy of the predictions of the root mean square infragravity wave heights based on the frequencies between 0.03 Hz–0.05 Hz is less favorable than that for the lower infragravity frequencies (compare Figs. 5 and 6) with generally less energy in the observations (panel A in Fig. 6) compared with the predictions (panel B in Fig. 6) during storm conditions. The corresponding over prediction of the total infragravity wave height (panel C) is predominantly related to the over prediction of the outgoing infragravity wave height (panel E) given the fact that the incoming infragravity wave height is well predicted (panel D).

Next, the bound wave height is examined. The bound infragravity wave variance in IDSB is calculated using the equilibrium solution:

$$S_b(x,\Delta f) = \int_{f_{c/o}}^{\infty} \int_{-\frac{\pi}{2}}^{\frac{\pi}{2}} \int_{-\frac{\pi}{2}}^{\frac{\pi}{2}} |C|^2 S(f+\Delta f,\alpha_1) S(f,\alpha_2) df d\alpha_1 d\alpha_2 \quad (4)$$

In which C is the coupling coefficient that determines the magnitude of the bound infragravity wave component resulting from two short wave components with a difference in frequency (Δf) and angle ($\alpha_2 - \alpha_1$) (refer to Reniers et al., 2002 for details).

The calculated root mean square wave heights are compared with the measurements using a bi-spectral analysis (Hasselmann and Munk, 1963) on the transformed surface elevation time series at the FRF array.

The overall comparison is good (Fig. 7); however the mean skill is equal to 0.5, which is significantly lower than obtained for the total root mean square infragravity wave height comparisons discussed above. The notably smaller skill can be explained by two factors; in the low regions, with bound rms long wave heights less than 0.02 cm, the predictions are slightly lower than the measurements, however this has a large effect on the mean skill due to the sensitivity of the skill to small measured values which appear in the denominator of Eq. (2). Another reason for the lower skill is due to the fact that the equilibrium solution (Eq. (4)) is not valid during the peak of the storm conditions when the ratio of root mean square incident wave height over water depth exceeds 0.3 (indicated by the yellow band in Fig. 7) and (some) wave breaking is present at the FRF array location. In that case the wave group forcing can no longer be considered as slowly varying resulting in an over prediction of the bound infragravity wave height (Battjes et al., 2004). Neglecting these data the comparison with the measured bound waves shows a good correlation, with a mean root mean square error of less than 2 cm.

The measured bound component explains typically 10–20% of the total infragravity wave height and never exceeds the 50% during this month (not shown). This result is consistent with earlier observations (e.g. Okihiro and Guza, 1995). Using the bound wave calculations only to estimate the infragravity conditions for ship motions can thus result in a significant underestimation of the infragravity wave height (compare Figs. 3 and 7).

In conclusion, the total root mean square infragravity wave height at the FRF array in the frequency range of 0.01 Hz–0.05 Hz is well predicted by the combined 1D–SWAN–IDSB modeling approach yielding a skill of O(0.8) thus explaining 80% of the variability present in the observations. This high skill includes both moderate incident wave conditions and storm conditions. Differences are mostly apparent in the 0.03 Hz–0.05 Hz frequency range of the infragravity wave conditions during storm conditions when the outgoing and total infragravity wave heights are over predicted. The mean direction and corresponding directional spreading for the outgoing infragravity waves are well predicted. And although the mean direction of the incoming infragravity waves is generally well predicted, the corresponding directional spreading is generally too broad.

The relatively short transformation distance of the frequency-directional short wave spectra at the offshore buoy location 3.5 km from the coast only allows for the verification of physical processes within SWAN that have quick time and spatial scales such as refraction, shoaling, triads and wave breaking and has therefore limited validity. For longer wave transformation distances other processes such as wave growth, bottom friction and Bragg scattering also become important. This is examined next.

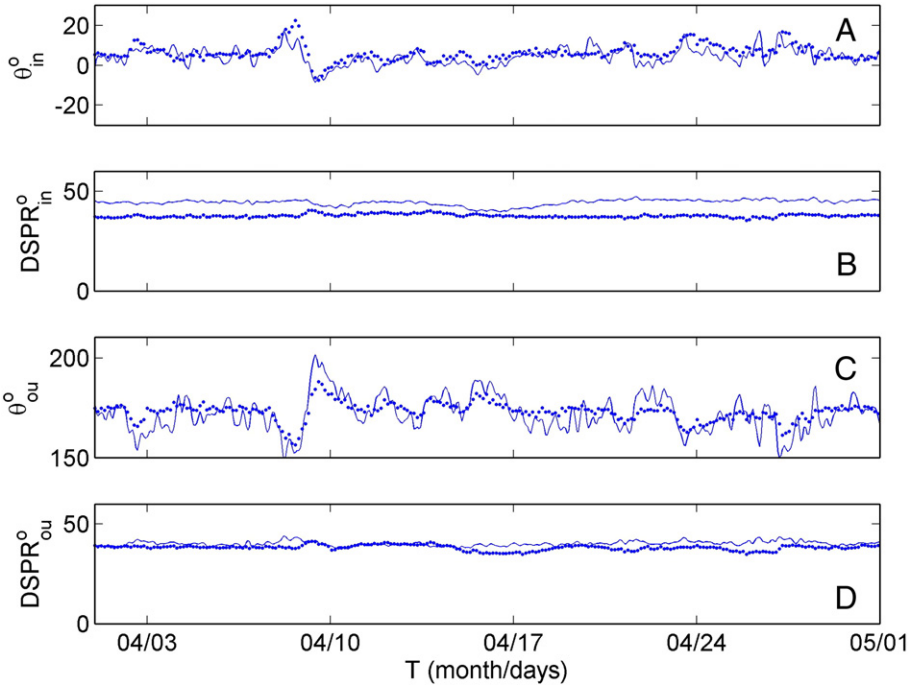

Fig. 4. Observed (dots) and predicted (solid lines) infragravity conditions during April 2005 at the 8 m-array location. Panel A: Mean direction of the incoming infragravity waves. Panel B: Directional spreading of incoming infragravity waves. Panel C: Mean direction of the outgoing infragravity waves. Panel D: Directional spreading of outgoing infragravity waves.

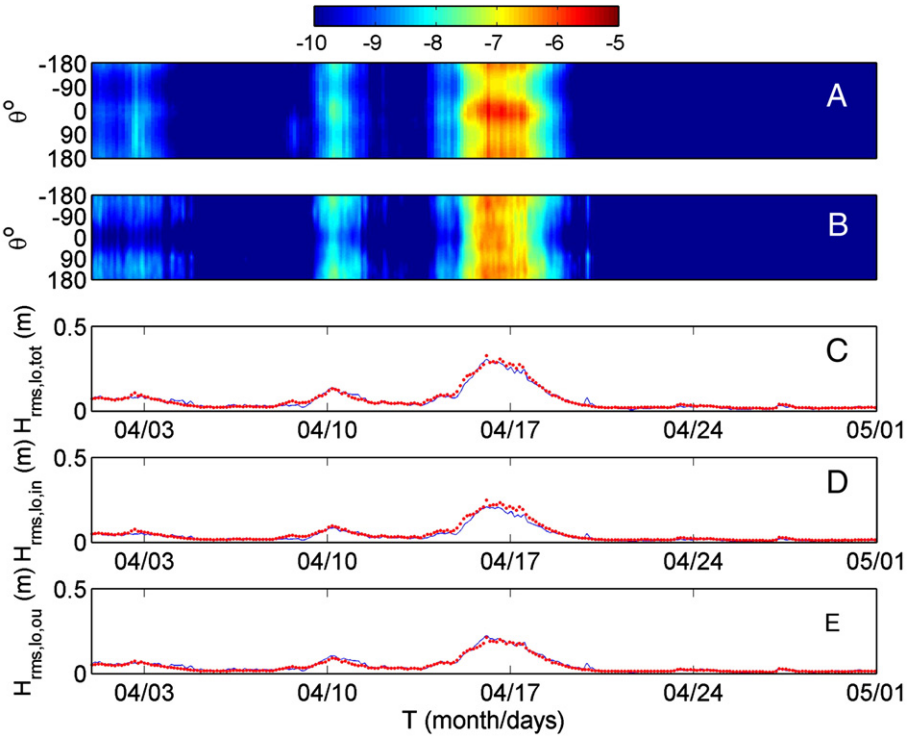

Fig. 5. Infragravity conditions during April 2005 at the 8 m-array location. Panel A: Observed 0.01 Hz – 0.03 Hz frequency-integrated directional infragravity spectra. Panel B: Similar for predicted directional infragravity spectra. Panel C: Observed (red dots) and predicted (solid line) total infragravity root mean square wave height. Panel D: Incoming infragravity root mean square wave height. Panel E: Outgoing infragravity root mean square wave height.

5. 2D–SWAN wave transformation

In the following the SWAN boundary conditions are obtained from a directional wave buoy (44014 operated by the National Data Bouy Centre) located at the shelf edge approximately 70 km from the coast (Fig. 8). The hourly short wave frequency-directional spectra are again estimated with the Maximum Entropy Method (MEM) (Lygre and Krogstad, 1986). The bathymetry data used in the 2D–SWAN

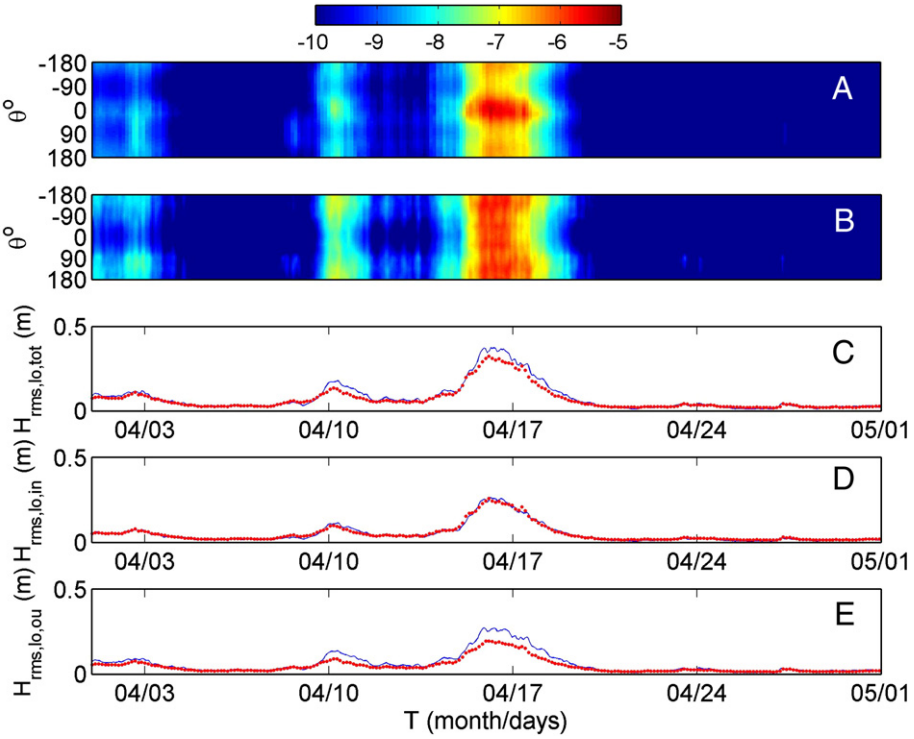

Fig. 6. Infragravity conditions during April 2005 at the 8 m-array location. Panel A: Observed 0.03 Hz – 0.05 Hz frequency-integrated directional infragravity spectra. Panel B: Similar for predicted directional infragravity spectra. Panel C: Observed (red dots) and predicted (solid line) total infragravity root mean square wave height. Panel D: Incoming infragravity root mean square wave height . Panel E: Outgoing infragravity root mean square wave height.

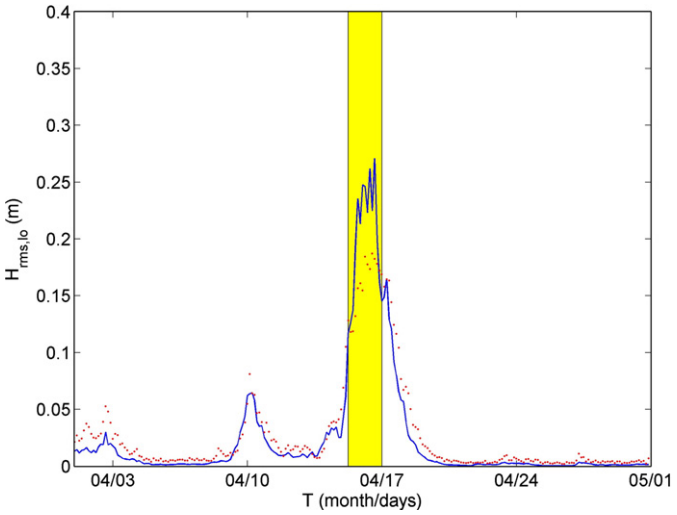

Fig. 7. Bound infragravity root mean square wave height based on the variance density spectra with frequency domain 0.01 Hz – 0.05 Hz computed with IDSB at 8 m-array location (solid line) and measured (red dots) at 8 m-array location during April 2005. Period when ratio of root mean square incident wave height over water depth exceeds 0.3 indicated in yellow.

calculations, derived from the National Ocean Service digital database and additional bathymetric surveys conducted during the DUCK94, is described by Ardhuin et al., 2001. Given the strong bathymetric variability (Fig. 8) a 2D–SWAN computation is warranted. To calculate the short wave frequency-directional spectra at the FRF location a nested computation is performed with a grid spacing of 0.015° for the largest domain, 0.005° for the intermediate domain and 0.0015° for the FRF domain (Fig. 8). The 2D–SWAN calculations are performed with the default settings presented earlier and now include wind input using the hourly mean wind speed and direction at the buoy location and white capping (Komen et al., 1984, 1994; Hasselmann, 1974) as well as quadruplets (Hasselmann et al., 1985). The directional resolution is 10° and 30 intervals with a logarithmic scale are used to describe the frequency domain between 0.05 Hz and 0.31 Hz. Computations with higher resolution in direction, frequency and space give minimal differences in the 2D–SWAN output.

2D–SWAN output at the 8 m FRF array is again compared with the observations showing good correspondence for Hm0 (skill = 0.84, $\varepsilon = 0.2$ m) and the mean frequency (skill = 0.81, $\varepsilon = 0.03$ Hz) with the largest mismatches at times of minimal wave energy. Moderate skill is obtained for the mean direction (skill = 0.3, $\varepsilon = 8°$) and directional spreading (skill = 0.66, $\varepsilon = 8°$) where the latter is persistently under predicted (Fig. 9). This is most likely a result of Bragg scattering effects, which are not included in SWAN, and are known to lead to significant broadening of the short wave directional distribution as swell waves propagate from the shelf edge to the nearshore (Ardhuin et al., 2003).

Next the short wave 2D–SWAN frequency-directional spectra are used as input for the IDSB calculations to compute the infragravity response at the 8 m FRF array location. Comparing the predicted response for the total infragravity wave height generally shows an over prediction (Fig. 10) with a mean skill of 0.47 and $\varepsilon = 5$ cm. Given the fact that the directional distribution of the incident waves is important in the forcing of the infragravity response (Herbers et al., 1994, 1995a) this is likely to affect the IDSB infragravity predictions in an adverse way. To examine this effect a smoothing filter is applied to the directional distribution of the short wave spectra calculated by SWAN to match the observed directional spreading. The filtered spectra are subsequently used by IDSB to calculate the infragravity response. This results in a considerable improvement increasing the skill to 0.7 and reducing ε to 3.0 cm (Fig. 10).

6. Discussion

The tidal range at Duck is in the order of 1 m. The influence of changes in the tidal elevation on the infragravity wave height calculated with IDSB has been examined by adding a set-up of 0.6 m during the peak storm conditions in the middle of April 2005. The calculated infragravity wave height at the FRF 8 m array did not change significantly due to this effect. The fact that the change in water level only marginally affects the outcome at the array location, in combination with the absence of a tidal signature in the measured infragravity wave heights, supports the present approach of ignoring the tidal variation in the infragravity computations at this site. This insensitivity to changes in the water level is a function of the local water depth, where significant variation in the infragravity wave heights can be present closer to the water line due to non-linear shoaling (e.g. Battjes et al., 2004). However, this effect is mostly absent in deeper water, which can be inferred from the expected amplitude increase for the infragravity waves shown below.

For the bound waves this increase is proportional to $h^{\frac{-5}{2}}$ (Longuet-Higgins and Stewart, 1962, 1964) yielding an O(15%) increase in infragravity wave height at the FRF array with a corresponding decrease of 0.5 m in the mean water level. For free infragravity waves this amplitude increase is proportional to $h^{\frac{-1}{4}}$ (Green's Law) resulting in a O(1%) increase in the infragravity wave height at the FRF array location. Given the fact that the most of the infragravity energy is free at this location (Herbers et al., 1994, 1995b) the sensitivity to changes in the water depth is expected to be small, provided the infragravity generation process within the surf zone is not affected by the changes in the mean water depth, discussed below.

At present all the incoming infragravity energy is expected to reflect at the beach. Given the fact that the beach at Duck is rather steep close to the water line, with a near constant slope in the order of 0.05, this is a valid assumption for most of the infragravity conditions present at Duck. However, during storm conditions infragravity

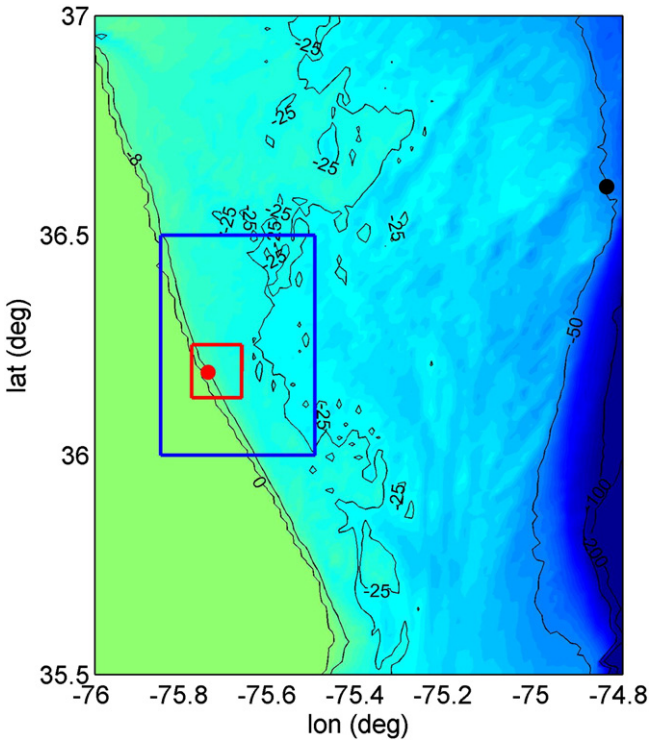

Fig. 8. Bathymetry (depth contours in m) and computational grid enclosures for nested 2D-SWAN computations. NDBC buoy 44014 indicated by the black marker. FRF 8 m-array indicated by the red marker.

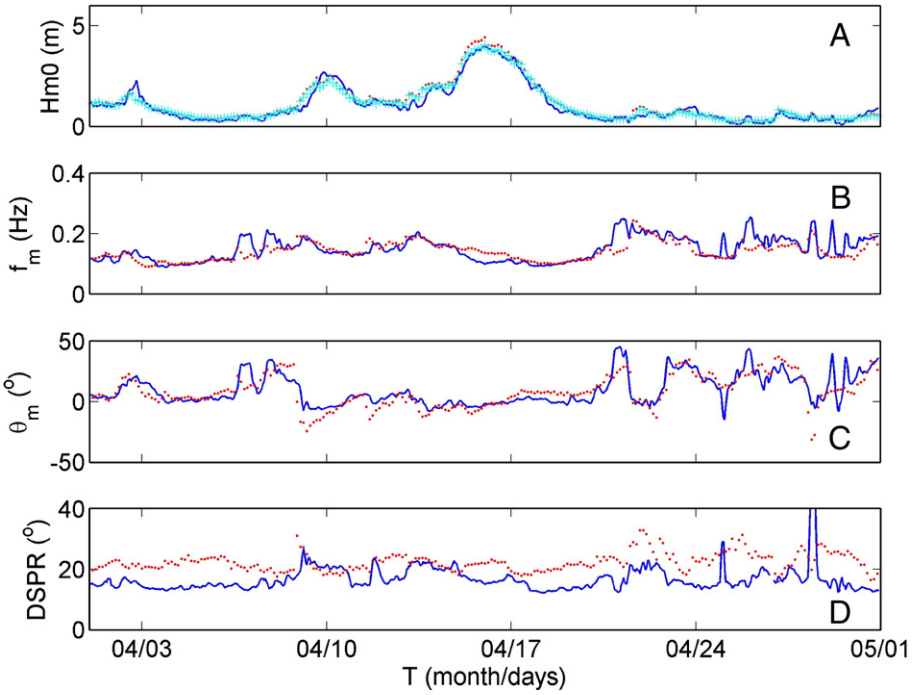

Fig. 9. Comparisons between 2D-SWAN output at 8.8 m water depth and FRF data published on the website at 8 m-array location. Panel A: Hm0 computed with SWAN (solid), FRF data (•) and a FFT computation at 8.8 m water depth (x). Panel B: Mean frequency computed with SWAN (solid) and FRF data (•). Panel C: Mean incidence angle (0° is shore normal) computed with SWAN (solid) and FRF data (•). Panel D: Circular root mean square spreading computed with SWAN (solid) and FRF data (•).

energy may be lost due to wave breaking in addition to bottom friction (van Dongeren et al., 2007). This especially holds for the higher infragravity frequencies for which the relative slope, i.e. the ratio of beach slope and wave surface slope given by:

$$\beta_H = \frac{h_x}{\omega}\sqrt{\frac{g}{H_{\mathrm{rms,lo,in}}}} \tag{6}$$

is lower, resulting in infragravity wave breaking and consequently smaller reflection coefficients. A rough estimate of β_H during the peak of the storm with the incoming root mean square infragravity wave height $H_{\mathrm{rms,lo,in}} = \mathrm{O}(25)\,\mathrm{cm}$, the bed slope near the water line $h_x = 0.05$, and the infragravity radial frequency $\omega = 2pi \cdot f_{\mathrm{lo}}$ yields a reflection coefficient of O(0.6) for $f_{\mathrm{lo}} = 0.05$ Hz (Battjes, 1974; van Dongeren et al., 2007). The reflection increases quickly with decreasing frequency and is expected to be of O(1.0) for frequencies less

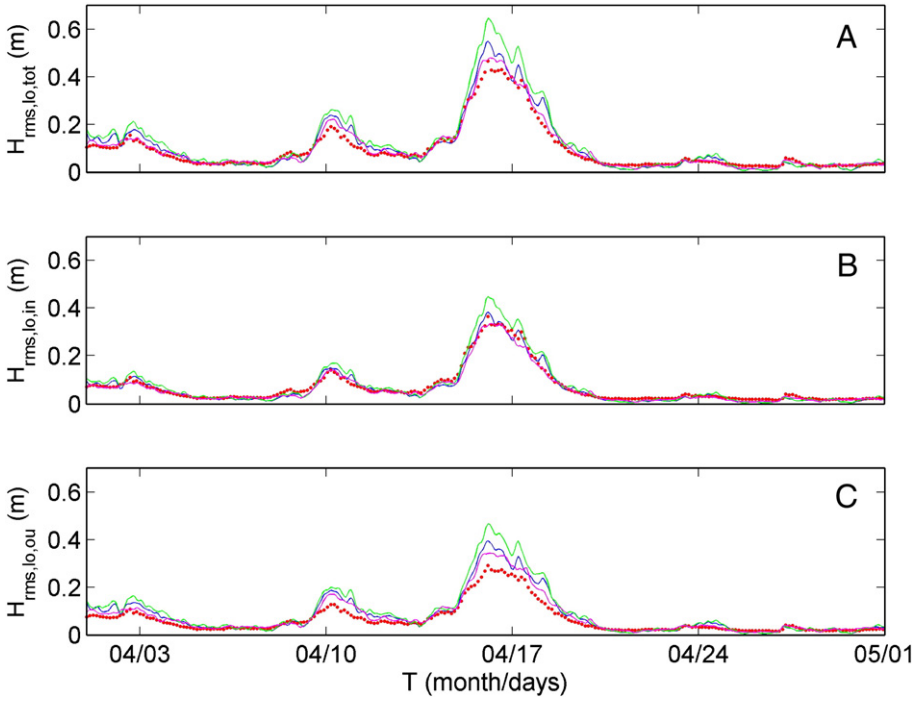

Fig. 10. Infragravity conditions during April 2005 at the 8 m-array location. Panel A: Observed (red dots) and predicted total infragravity root mean square wave height for 2D-swan (green line), directionally smoothed 2D-swan (blue) and 1D-swan (magenta). Panel B: Similar for the incoming infragravity root mean square wave height. Panel C: Similar for the outgoing infragravity root mean square wave height.

than 0.04 Hz under these conditions. Therefore, only the infragravity response at higher infragravity frequencies will be affected. This is consistent with the presently obtained results where the low frequency infragravity waves are better predicted than the high frequency infragravity waves (compare Figs. 5 and 6). However the present data set does not allow for a complete validation of the infragravity breaking mechanism and the analysis outlined above is only an indication of the potential importance of dissipation due to infragravity wave breaking. The analysis does suggest that the reflection of infragravity waves near the water line is close to unity, consistent with the results obtained by Sheremet et al. (2002), and supports the use of a fully reflective boundary condition in the model.

In cases where the beach slope changes with the mean water level, the reflection coefficient becomes a function of the tidal elevation and as such the infragravity response at deeper water is also expected to be tidally modulated. Tidal modulation of the infragravity response, which is mostly absent at the Duck site, has been observed at other locations (Okihiro and Guza, 1995), and was recently attributed to a transfer of infragravity wave energy to the incident waves through non-linear triad wave interactions (Thomson et al., 2006). This transfer of energy is dependent on the slope of the profile in the shallowest part, with water depths less than 1 m, where a mild slope creates a larger transfer than a steep slope. Tidal modulation in the infragravity response then results from changes in the average slope with tidal elevation. In those cases, the tidal elevation and changes in the reflection coefficient resulting from either non-linear wave interaction (Thomson et al., 2006) or infragravity wave breaking (van Dongeren et al., 2007) should be included in the infragravity response calculations.

The bottom profile used in this study has different sources. The profile from the shore to the 8-meter array is unchanged compared to the study by Reniers et al. (2004) and originates from the Sandy Duck experiment from 1997. The bathymetry that is used to determine the profile from the buoy to the array is based on surveys done in 1999 and 2000. These data are combined into one bottom profile with a match at 8.8 m water depth corresponding to the location of the most offshore FRF array sensor. At the array location small differences between the different surveys can be distinguished. The influence of these small bathymetry changes (0.2 m) on the results has not been examined, but is not expected to be significant given the insensitivity to the changes in the mean water depth discussed above.

To assess the effect of differences in the profile from the FRF array to shore, the infragravity response is calculated using a profile from a survey performed in March 2005. Although this profile differs in the surf zone compared with 1997 profile, both the beach slope and offshore slope are similar (Fig. 1). The differences in the calculated infragravity response for the month of April at the FRF 8 m array for the 2005 profile are O(1) cm compared with the results obtained with the 1997 profile. This shows that the infragravity response at an intermediate depth of 8.4 m at Duck is insensitive to the changes in the surfzone bottom profile, provided these changes do not affect the reflection coefficient.

The bathymetry in the infragravity modeling approach has been assumed to be alongshore uniform. Even though alongshore variability is often present in the surfzone at Duck (Lippmann and Holman, 1989), their effect on the infragravity response is generally limited (Reniers et al., 2002; van Dongeren et al., 2003), which is supported by the present results. In the case of strong bathymetric variability within the surfzone, a coupling between infragravity waves and the underlying bathymetry may be present affecting the infragravity response at certain infragravity frequencies (Reniers et al., 2006).

7. Conclusions

The spectral model SWAN and the linear model IDSB have been combined to calculate infragravity wave heights at a water depth of 8.4 m. 1D–SWAN has been used to translate the short wave directional frequency spectra obtained by a Waverider buoy located 3.5 km from the coast at 18 m water depth to 8.8 m water depth. The 1D–SWAN predicted significant wave height, mean wave period, mean wave direction and directional spreading show good agreement with the measured wave data.

Next, IDSB has used these frequency-directional spectra to calculate the root mean square infragravity wave heights at the FRF 8 m array based on the variance densities between 0.01 Hz–0.05 Hz. The comparison of the measured and the computed root mean square infragravity wave heights show a mean skill of O(0.8) at 8.4 m water depth. The infragravity response at the FRF array is mostly insensitive to changes in the water depth, which is attributed to the fact that the FRF array is well outside the surfzone and that the infragravity generation processes within the surfzone are not affected by changes in the tidal elevation.

The comparison of the infragravity waves in the lower frequencies (0.01 Hz–0.03 Hz) shows a better agreement than the comparison in the higher frequencies (0.03 Hz–0.05 Hz), especially during storm conditions. In general the outgoing infragravity waves are over predicted suggesting the omission of a dissipative process within the IDSB model such as the energy dissipation due to infragravity wave breaking as outlined by van Dongeren et al. (2007) or the transfer of infragravity wave energy to the incident waves through non-linear triad wave interactions (Thomson et al., 2006).

2D–SWAN has been used to translate the frequency-directional spectra obtained from a directional wave buoy located at the shelf edge 70 km from the coast to the FRF array location. Good agreement is obtained for the significant wave height and mean wave period. However, the corresponding directional spreading is persistently under predicted, most likely due to the absence of Bragg scattering effects in SWAN. As a result the observed infragravity wave heights are over predicted with a mean skill of 0.47. Accounting for the short wave spreading mismatch increases the model skill to 0.7.

SWAN–IDSB is a very compatible combination of wave models, where the 2D spectra produced by SWAN can be used in IDSB without much adjustment. To calculate one month of data takes approximately 24 h, which is significantly faster than can be obtained with more complex models such as Boussinesq (Chen et al., 2003 among others). This allows for the calculation of the infragravity conditions for long periods of time (i.e. multiple years), which subsequently can be used as boundary conditions for downtime computations due to unacceptable ship motions induced by the infragravity motions, and to develop infragravity wave height design criteria, which can be used for the design of nearshore tanker offloading facilities. Also, the fact that SWAN can be easily coupled to a global wave model allows for rapid assessments of infragravity conditions along coasts similar to Duck with a relatively steep and constant bed slope at the shoreline and low tidal water level modulation, in combination with moderate incident wave conditions. Nevertheless, we anticipate that future applications of this approach would necessarily be accompanied by a validation study in which model predictions are validated against a carefully measured set of wave measurements at the location of interest, as is normal in assessing the accuracy of long-term data bases produced from numerical models.

Acknowledgement

Data used in this study are provided by the Field Research Facility of the US Army Engineer Waterways Experiment Station's Coastal Engineering Research Centre. Data from buoy 44014 are provided by the National Data Buoy Centre (available online at http://www.ndbc.noaa.gov). Accessibility and permission to use these data is appreciated very much. A collaboration of Technical University Delft departments of Fluid Mechanics and Offshore Engineering together with the Shell International Exploration and Production Metocean

Department has funded this work. We thank Fabrice Ardhuin and Tom Herbers for providing us with the 2D shelf bathymetry based on the Bathymetric data obtained from the U. S. National Oceanographic Data Centre. We thank Bob Guza and an anonymous reviewer or providing us with valuable comments that have resulted in an improved paper.

Appendix A

To calculate the frequency-directional distribution of the infragravity waves the Maximum Likelihood Estimator (MLE, Davis and Regier (1977), Pawka (1983)) is applied in the following way. First the wave number directional spectrum, $E(k,\theta)$, for a given frequency f is estimated by:

$$E(f,k,\theta) = D\left[\sum_{n=1}^{N}\sum_{m=1}^{N} X_{nm}^{-1}(f)e^{-(ik\sin\theta(y_m-y_n)\ +\ ik\cos\theta(x_m-x_n))}\right] \quad \text{(A1)}$$

Where x_m and y_m correspond to the cross-shore and along shore location of sensor m within the FRF 8 m array. $X_{nm}^{-1}(f)$ is the nm component of the inverse cross-spectral matrix at frequency f obtained from the surface elevation cross-spectra at sensor locations n and m, and D is a scaling coefficient. Owing to different instrument locations, each cross-spectral value, $X_{nm}(f)$, was normalized such that the diagonals of the cross-spectral matrix are unity prior to the inversion (MacMahan et al., 2004). Spectral estimates with 40 degrees of freedom (frequency resolution of 0.0078 Hz) were generated from demeaned, quadratically detrended 2.75 hour records of surface elevation calculated from the pressure signals using linear wave theory.

The rationale behind the calculation of the wave number spectrum is the presence of bound long waves where the wave length is not determined by dispersion relation but dictated by the difference wave number of the incident waves forcing the bound long wave. Integrating the wave number spectrum yields the frequency-directional infragravity energy spectrum, $E(f,\theta)$. Further integration over the infragravity frequency interval then yields the directional spectra, $E(\theta)$, shown in Figs. 3, 5 and 6.

Given the generally broad directional distribution of infragravity wave spectra (Herbers et al., 1995b) no attempt was made to use the Iterative Maximum Likelihood Estimator (IMLE, Pawka, 1983). And the fact that the MLE is designed for a homogeneous wave field whereas the reflection at the shore line results in standing infragravity wave patterns is overcome by choosing relatively broad frequency bandwidths (Herbers et al., 1995b).

References

Apotsos, A., Raubenheimer, B., Elgar, S., Guza, R.T., 2008. Testing and calibrating parametric wave transformation models on natural beaches. Coast. Eng. 55 (3), 224–235.

Ardhuin, F., Herbers, T.H.C., O'Reilly, W.C., 2001. A hybrid Eulerian–Lagrangian model for spectral wave evolution with application to bottom friction on the continental shelf. JPO 31, 1498–1516.

Ardhuin, F., Herbers, T.H.C., Jessen, P.F., O'Reilly, W.C., 2003. Swell transformation across the continental shelf. Part II: Validation of a spectral energy balance equation. J. Phys. Oceanogr. 33, 1940–1953.

Battjes, J.A., 1974. Surf similarity. Proceedings of the 14th International Conference on Coastal Engineering. ASCE, pp. 466–480.

Battjes, J.A., Bakkenes, H.J., Janssen, T.T., van Dongeren, A.R., 2004. Shoaling of subharmonic gravity waves. J. Geophys. Res. 109 (C02009).

Biesel, F., 1952. Equations generales au second ordre de la houle irreguliere. Houille Blanche 7, 372–376.

Booij, N., Ris, R.C., Holthuijsen, L.H., 1999. A third generation model for coastal regions, part I: Model description and validation. J. Geophys. Res. 104, 7649–7666.

Chen, Q., Kirby, J.T., Dalrymple, R.A., Shi, F., Thornton, E.B., 2003. Boussinesq modeling of longshore currents. J. Geophys. Res. 108 (C11), 3362.

Davis, R.E., Regier, L.A., 1977. Methods for estimating directional wave spectra from multi-element arrays. J. Mar. Res. 35, 453–477.

Eldeberky, Y., Nonlinear transformation of wave spectra in the nearshore zone. PhD. Thesis, Dept. of. Eng., Delft Univ. of Technology, Delft, The Netherlands, 1996.

Gallagher, E.L., Elgar, S., Guza, R.T., 1998. Observations of sand bar evolution on a natural beach. J. Geophys. Res. 103, 3203–3215.

Hasselmann, K., Munk, W., MacDonald, 1963. Bispectra of ocean waves. In: Rosenblatt, M. (Ed.), Time series Analysis. Wiley, New York, pp. 125–139.

Hasselmann, K., Barnett, T.P., Bouws, E., Carlson, H., Cartwright, D.E., Enke, K., Ewing, J.A., Gienapp, H., Hasselmann, D.E., Kruseman, P., Meerburg, A., Muller, P., Olers, D.J., Richter, K., Sell, W., Walden, H., 1973. Measurements of wind–wave growth and swell decay during the Joint North Sea Wave Project (JONSWAP). Dtsch. Hydrogr. Z. Suppl. 12 A8.

Hasselmann, K., 1974. On the spectral dissipation of ocean waves due to whitecapping. Boundary - Layer Meteorol. 6 (1–2), 107–127.

Hasselmann, S., Hasselmann, K., Allender, J.H., Barnett, T.P., 1985. Computations and parameterizations of the nonlinear energy transfer in a gravity wave spectrum. Part II: Parameterizations of the nonlinear transfer for application in wave models. J. Phys. Oceanogr. 15 (11), 1378–1391.

Herbers, T.H.C., Elgar, S., Guza, R.T, 1994. Infragravity-frequency (0.005–0.05 Hz) motions on the shelf, part I, Forced waves. J. Phys. Oceanogr. 24, 917–927.

Herbers, T.H.C., Elgar, S., Guza, R.T, 1995a. Generation and propagation of infragravity waves. J. Geophys. Res. 100, 24, 863–24, 872.

Herbers, T.H.C., Elgar, S., Guza, R.T., O'Reilly, W.C., 1995b. Infragravity-frequency (0.005–0.05 Hz) motions on the shelf, II, free waves. J. Phys. Oceanogr. 25, 1063–1079.

Komen, G.J., Hasselmann, S., Hasselmann, K., 1984. On the existence of a fully-developed wind–sea spectrum. J. Phys. Oceanogr. 14, 1271–1285.

Komen, G.J., Cavaleri, L., Donelan, M., Hasselmann, K., Hasselmann, S., Janssen, P.A.E.M., 1994. Dynamics and Modelling of Ocean Waves. Cambridge University Press. 532 pp.

Kuik, A.J., van Vledder, G.Ph, Holthuijsen, L.H., 1988. A method for routine analysis of pitch-and-roll buoy wave data. J. Phys Ocean. 18, 1020–1034.

Longuet-Higgins, M.S., Stewart, R.W., 1962. Radiation stress and mass transport in surface gravity waves with application to "surf beats". J. Fluid Mech. 29, 481–504.

Longuet-Higgins, M.S., Stewart, R.W., 1964. Radiation stresses in water waves: a physical discussion, with applications. Deep-Sea Res. 11, 529–562.

Lippmann, T.C., Holman, R.A., 1989. Quantification of sand bar morphology: a video technique based on wave dissipation. J. Geophys. Res. 94, 995–1011.

Lygre, A., Krogstad, H.E., 1986. Maximum entropy estimation of the directional distribution in ocean wave spectra. J. Phys. Oceanogr. 16, 2052–2060.

MacMahan, J., Reniers, A.J.H.M., Thornton, E.B., Stanton, T.P., 2004. Infragravity rip-current pulsations. J. Geophys. Res. 109 (C01033). doi:10.1029/2003JC002068.

McCall, R.T., J.S.M. van Thiel de Vries, N.G. Plant, A.R. van Dongeren, J.A. Roelvink, D.M., 2009. Thompson and A.J.H.M. Reniers, two-dimensional hurricane overwash and erosion modeling at Santa Rosa Island, submitted to *Coastal Eng.*

Munk, W.H., 1949. Surf beats. Eos Trans. AGU 30, 849–854.

Naciri, M., Buchner, B., Bunnik, T., Huijsmans, R., Andrews, J., 2004. Low frequency motions of LNG carriers in shallow water. Proceedings Offshore Mechanics & Arctic Engineering Conference.

Okihiro, M., Guza, R.T., 1995. Infragravity energy modulation by tides. J. Geophys. Res. 100 (C8) 16,143–16,148.

Pawka, S.S., 1983. Island shadows in wave directional spectra. J. Geophys. Res. 88 (C4), 2579–2591.

Reniers, A.J.H.M., van Dongeren, A.R., Battjes, J.A., Thornton, E.B., 2002. Linear modeling of infragravity waves during Delilah. J. Geophys. Res. 107 (C10), 3137. doi:10.1029/2001JC001083.

Reniers, A.J.H.M., Thornton, E.B., Stanton, T.P., Roelvink, J.A., 2004. Vertical flow structure during Sandy Duck: observations and modeling. Coast. Eng. 51, 237–260.

Reniers, A.J.H.M., MacMahan, J., Thornton, E.B., Stanton, T.P., 2006. Modelling infragravity motions on a rip-channel beach. Coast. Eng. 53, 209–222.

Ris, R.C., Booij, N., Holthuijsen, L.H., 1999. A third-generation wave model for coastal regions, Part II: Verification. J. Geophys. Res. 104, 7667–7682.

Roelvink, J.A., Stive, M.J.F., 1989. Bar generating cross-shore flow mechanisms on a beach. J. Geophys. Res. 94, 4785–4800.

Roelvink, J.A., Surfbeat and its effect on cross-shore profiles, PhD thesis, Delft Univ. of Technol., Netherlands, 1993.

Roelvink, J.A., Reniers, A.J.H.M., van Dongeren, A.R., van Thiel de Vries, J.S.M., McCall, R.T., Lescinski, J., 2009. Modelling storm impacts on beaches, dunes and barrier islands. Coastal Eng. 56 (11–12), 1133–1152.

Sand, S.E., 1982. Long waves in directional seas. Coast. Eng. 6, 195–208.

Sheremet, A., Guza, R.T, Elgar, S., Herbers, T.C., 2002. Observations of nearshore infragravity waves: 1. Seaward and shoreward propagating components. J. Geophys. Res. 107 (C8), 3095.

Thomson, J., Elgar, S., Raubenheimer, B., Herbers, T.H.C., Guza, R.T., 2006. Tidal modulation on infragravity waves via nonlinear energy losses in the surfzone. Geophys. Res. Lett. 33 (L05601). doi:10.1029/2005GL025514.

Tucker, M.J., 1950. Surfbeats: sea waves of 1 to 5 minutes' period. Proc. R. Soc. Lond., Ser. A 202, 565–573.

Ursell, F., 1952. Edge waves on a sloping beach. Proc. R. Soc. Lond., Ser A 314, 79–97.

van der Molen, 2006. Behaviour of Moored Ships in Harbours, PhD thesis, Delft University of Technology, 140 pp.

van der Molen, W., Monardez, P., van Dongeren, A.R., 2006. Numerical simulation of long-period waves and ship motions in Tokakomai Port, Japan. Coast. Eng. J. 48, 59–79.

van Dongeren, A., Reniers, A., Battjes, J., Svendsen, I., 2003. Numerical modeling of infragravity wave response during Delilah. J. Geophys. Res 108, 4-1.

van Dongeren, A., Battjes, J., Janssen, T., van Noorloos, J., Steenhauer, K., Steenbergen, G., Reniers, A., 2007. Shoaling and shoreline dissipation of low-frequency waves. J. Geophys. Res. 112 (C02011).

van Gent, M.R.A., 2001. Wave runup on dikes with shallow foreshores. J. Waterways, Ports and Coast. Ocean Eng. 127 (5), 254–262.

van Thiel de Vries, J.S.M., van Gent, M.R.A., Reniers, A.J.H.M., Walstra, D.J.R., 2008. Analysis of dune erosion processes in large scale flume experiments. Coastal Eng. 55, 1028–1040. doi:10.1016/j.coastaleng.2008.04.004.